

# On the Sensitivity of Protein Data Bank Normal Mode Analysis: An Application to GH10 Xylanases

Monique M. Tirion\*

*Physics Department, Clarkson University, Potsdam, New York 13699-5820, USA*

Protein data bank entries obtain distinct, reproducible flexibility characteristics determined by normal mode analyses of their three dimensional coordinate files. We study the effectiveness and sensitivity of this technique by analyzing the results on one class of glycosidases: family 10 xylanases. A conserved tryptophan that appears to affect access to the active site can be in one of two conformations according to X-ray crystallographic electron density data. The two alternate orientations of this active site tryptophan lead to distinct flexibility spectra, with one orientation thwarting the oscillations seen in the other. The particular orientation of this sidechain furthermore affects the appearance of the motility of a distant, C terminal region we term the mallet. The mallet region is known to separate members of this family of enzymes into two classes.

## I. INTRODUCTION

### A. Protein NMA

Protein atomic coordinates, determined by a variety of techniques, are deposited in the Protein Data Bank (PDB) [1]. The PDB coordinate files permit determination of numerous physical qualities, including charge distribution at a given pH, mass distribution, principal axes of rotation as well as the internal symmetry axes that characterize each object's flexibility spectrum. Internal symmetry is determined by normal mode analysis (NMA), a technique first applied to protein structures in the 1980s after the first generations of (classical) protein force fields matured [2–4]. Go [2] and Levitt [5] independently formulated the eigenvector equations in torsional angle space while Brooks and Karplus [3] studied the vibrational response in Cartesian space.

As originally formulated, protein NMA requires an energy minimization to bring the PDB coordinates to a local energy minimum along the force field characterizing the object's energy surface [4]. This necessarily distorts the PDB coordinates away from the experimentally determined values and precludes the possibility of a true PDB-NMA. Ben-Avraham introduced the use of a (Hookean) potential energy function, one that is a minimum at the outset, to model inter-monomer interactions in F-actin so as to compute the atomic-based dispersion spectrum of this polymer [6]. We then generalized this formulation to model a protein's intra-monomer interactions, effectively introducing the field of PDB-NMA [7]. As then formulated, PDB-NMA necessarily retains proper molecular topology: no distortions of bond lengths or bond angles away from PDB values are allowed due to the use of dihedral degrees of freedom. That initial formulation examined solely the packing constraints of nonbonded van der Waal interactions, while current work incorporates restoring potentials associated with each dihedral degree of freedom as well [8, 10].

As an alternative to dihedral-based PDB-NMA, various formulations using Cartesian coordinates have been presented. These are generally referred to as Elastic Network Models (ENM), and include the popular Anisotropic Network Models (ANM) and Gaussian Network Models (GNM) [11, 12]. These alternative approaches to dihedral-based PDB-NMA rely on structural coarse-graining, such as the use of a single coordinate per residue. While this permits analyses of vast molecular assemblies such as ribosomes, topological constraints are necessarily sacrificed. (Even when formulated with full-atomic coordinates, i.e. no coarse-graining, the absence of bond-length and bond-angle constraints in ENMs will not maintain standard molecular topology.) A recent formulation, Torsional Network Model (TNM), makes use of any suitable potential energy function and projects the Cartesian degrees of freedom onto dihedral coordinates in order to preserve topology. Recent reviews summarize the relative merits of dihedral-based PDB-NMA, ENM and TNM [8, 9].

While the internal symmetry axes of each PDB entry are of interest in and of themselves, as I try to demonstrate here, often modal analyses are used to extend or enhance trajectories computed by Molecular Dynamics (MD). Temporal trajectories, necessarily non-equilibrium pathways, are not well modeled by NMA for two reasons. NMA is valid only near energy minima and assumes a harmonic or linear response to perturbations. Efforts to better model the nonlinear aspects of force fields has led to the use of various Principal Orthogonal Decomposition (POD) algorithms, such as

---

\*Electronic address: mmtirion@clarkson.edu

Principal Component Analysis (PCA) and Singular Value Decomposition (SVD), where eigenvectors are projected out of suitably long-time MD trajectories [2, 14]. The degree of overlap between eigenvectors derived from NMA and POD is still the basis of investigation [15].

Here we continue to explore the usefulness, range of validity as well as sensitivity of dihedral-based PDB-NMA [10]. Since no structure-distorting energy minimizations are required, we are able contrast the spectra of structures that differ only slightly, such as the two isoforms of the same molecule. To ascertain the significance of any difference, we will compare the flexibility characteristic of the same molecule, but solved in a different crystal form and also in the presence and absence of bound ligand. We also examine the computed flexibility spectrum of an evolutionary distant but structurally similar sample of the same enzyme.

We find that PDB-NMA provides detailed, precise, rapid, and reproducible predictions of flexibility signatures of PDB entries. Our investigation on the flexibility characteristics of one class of enzymes within the Carbohydrate Active Enzyme (CAZy) database, the glycoside hydrolase family 10 (GH10) xylanases, provides a mechanistic rationale for the distribution of experimental temperature factors, demonstrates how stability of key residues is maintained in the face of thermal perturbation, indicates the degree of homology in the flexibility patterns across enzymes with closely similar architecture, and identifies regions with distinct flexibility patterns. These analyses suggest that studying a protein’s flexibility characteristics is helpful in order to understand and categorize the unique consequences of the overall three dimensional conformation of each PDB entry.

## B. Protein System Studied

Xylanases hydrolyze xylan, wood sugar polysaccharides of the aldopentose xylose. Unlike planar glucose polysaccharides, xylan adopts a three-fold, left-handed helical conformation and is often decorated by a variety of branched side chains. Xylanases are produced by a wide variety of organisms from bacteria to fungi, protozoa and even gastropods who use xylose as a primary carbon source. As each organism targets different sources of plant hemicelluloses and since xylan presents as complex, branched heteropolysaccharides with structures varying between plant species, xylanases come with differing sensitivities to structural details of substrate and environmental cues. Various commercial enterprises, such as the paper and pulp industries, wine production and brewing, textile and baking industries to name a few, process the hemicelluloses found in plants. This explains the intense interest and the large numbers of X-ray crystallographic structures involving xylanases to study their structures and activities under various conditions of temperature, pH, alkalinity etc. [16]

Xylanases belonging to the GH10 family of glycosidases possess a classic  $(\alpha/\beta)_8$  or TIM barrel fold. The central barrel, consisting of eight parallel  $\beta$ -strands, flares out from a narrower “stability face” at the N-terminal ends to a wider “catalytic face” at the C-terminal ends of the  $\beta$ -strands [17]. Xylanase GH10 members display their greatest diversity in structure in the positions and loop architecture at the open, catalytic face, where the substrate binding groove and active site are situated [16].

Family 10 xylanases hydrolyse the internal (1,4) glycosidic bonds linking xylose moieties using two conserved glutamate residues, one acting as a general acid/base and the other as a nucleophile. As one glutamate is situated at the C-terminal end of  $\beta$ -strand 4 and the other at the end of  $\beta$ -strand 7, these xylanases belong to the 4/7 superfamily of TIM barrel folds (also known as clan GH-A). Hydrolysis proceeds via a double displacement mechanism that retains the anomeric configuration of the glycosidic oxygen [18]. This reaction scheme involves formation of a covalently bound, glycosyl-enzyme intermediate, enabling these xylanases to perform transglycosylation (polymerization) as well as hydrolysis (depolymerization) reactions [19, 20].

The substrates of family 10 xylanases bind in deep grooves to enable proper orientation and distortion of the sugar moieties to strain the glycosidic bond prior to cleavage. These binding grooves extend away from the catalytic glutamate residues, with “pockets” able to accommodate consecutive sugar moieties on both sides of the cleavage site. Each “subsite” is labeled: ...-2,-1,1,2,..., with negative subsites situated at the non-reducing, glycone end of the scissile bond, and positive sites situated on the reducing, aglycone side. The glycosidic bond between the xylose residues bound at subsites -1 and 1 is cleaved. Family 10 xylanases possess no fewer than 3 subsites, and possibly as many as 6 or 7 [16].

Family 10 xylanases possess numerous conserved residues besides the catalytic glutamates, including three tryptophans that form an “aromatic cage” about subsite -1. One tryptophan in particular, situated in the loop after  $\beta$ -strand 8 and present in all family 10 xylanases, is unique, with no equivalent aromatic residue found in any other 4/7 superfamily of enzymes [21]. Experimental studies demonstrate that mutation or inactivation by oxidation of this tryptophan disables enzyme activity in xylanases [22, 23]. An early X-ray crystallographic study of another glycosidase, lysozyme, demonstrated that the oxidation of its active site tryptophan inhibits the binding of substrate and enzyme activity, and results in a rotation of the indole moiety [24]. Recent X-ray crystallographic studies on family 10 xylanases demonstrate that the orientation of the active site tryptophan in these enzymes correlates with

the presence or absence of ligand in the active site [21]. We were interested to observe whether PDB-NMA could detect the effect of the orientation of this residue in the vibrational signatures of these enzymes. In fact, we observe a clear difference, with one orientation of the active site tryptophan leading to a distinct dampening of the oscillatory motion.

## II. TECHNIQUE

### A. Method

To compute eigenspectra and eigenmodes we maintained the same algorithm and parameterization, ATMAN, recently introduced for PDB-NMA and described in detail in [10]. The input data include the atomic coordinates,  $\vec{r}_i$ , and identities of every entry,  $i$ , in the PDB listing. Mainchain amide hydrogens were built in using the program *reduce* [25]. We used standard values for van der Waals radii  $R_{vdW_i}$ , atomic masses,  $m_i$ , and van der Waals energy well-depths,  $\epsilon_i$ , for each atom type (Table I).

In addition to these atom-specific parameters, two additional inputs are required: **the cut-off distance,  $D$  that is added to the sum of the van der Waal radii ( $R_{vdW}$ ) for nonbonded interactions between atom pairs more than three-bond lengths apart**, as well as a stiffness constraint,  $k$ , on the sidechain dihedral  $\chi$  bonds. As shown in [10], large values of  $D$  result in vast numbers of nonbonded interactions (NBI) and lead to eigenspectra that differ substantially from those obtained using energy-minimized structures. Rather than obtain the characteristic “soft” responses in the eigenspectra frequency range  $1 - 250 \text{ cm}^{-1}$ , a large value of  $D$  in ATMAN yields a very stiff signature extending from  $1 - 40 \text{ cm}^{-1}$ . To obtain optimal fits of the eigenspectra, therefore, we maintained a value of  $D$  equal to  $1.6 \text{ \AA}$ . To eliminate instabilities in the diagonalization of the normal mode equations caused by weakly bound surface sidechains, we used a uniform dihedral stiffness constant of  $0.1 \text{ kcal/mol}$ . Like the atom-specific parameters, both  $D$  and  $k$  were maintained to fixed values throughout these analyses (Table I).

#### List of fixed ATMAN parameters

Atom	<u>RvdW</u>	mass	$\epsilon$
H	1.10	1.008	0.001
O	1.60	15.999	0.18479
N	1.65	14.007	0.41315
C	1.85	12.011	0.07382
A, B, G	1.75	12.011	0.03763
S	1.85	32.064	0.07382
<b>D</b>	<b>1.6 Å</b>		
<b>k</b>	<b>0.1 kcal/mol</b>		
<b>T</b>	<b>180K</b>		

TABLE I: H refers to hydrogen atoms, O to oxygen atoms, N to nitrogen atoms, C to tetrahedral carbons while A, B, and G refer to trigonal carbons and S refers to sulfur atoms. The van der Waals radii are given in Angstroms, masses are in daltons, and epsilons are in kcal/mol. The atomic data are from [26, 27]. The cutoff distance,  $D$ , and the dihedral bond stiffness constant,  $k$ , were as in [10]. All RMSD were computed at 180K.

In order to reestablish the overall energy scale of the computed eigenspectra *one adjustable* parameter,  $C$ , was necessary to analyze each PDB entry. Just as proteins across all classes and sizes obtain predictable mass per unit volume measures (density), proteins also obtain universal eigenfrequency spectra with predictable distributions, especially of slow modes [28]. We see, for example, both experimentally as well as within the NMA predictions, a distinct peak at  $25 \text{ cm}^{-1}$  that seems to be due to the inter-packing constraints of secondary elements [10]. This peak, corresponding to vibrations occurring at the  $1.3 \text{ psec}$  time scale, does not correspond to the slowest motions observed by NMA, which occur on the  $1 - 5 \text{ cm}^{-1}$  or  $30 - 7 \text{ psec}$  level, and which seem to be driven by nonlocal NBIs. We use

the observation that the number of computed modes with eigenfrequencies under  $20\text{ cm}^{-1}$  corresponds to 14% of all modes, to adjust the overall scale factor,  $C$ , for the PDB-NMA of each PDB entry.

To visualize the motion described by each eigenfrequency an amplitude of activation,  $\alpha_i$  must be selected for each mode  $i$ . Typically this is achieved using classical conservation of energy considerations: each normal mode obtains a time-averaged potential energy of  $\frac{1}{2}k_B T$  above the value at NS ( $k_B$  is Boltzmann’s constant and  $T$  is the absolute temperature). This gives  $\alpha_i^2 = 2k_B T/w_i^2$  [4]. We chose a value of  $T = 180\text{K}$  as experiments indicate that only below this temperature protein motility spectra may be modeled as simple harmonic oscillations [29].

## B. PDB entries analyzed

According to the CAZy database the X-ray crystallographic structures of 37 GH10 xylanases are currently deposited at the PDB. We report here on the PDB-NMAs of 5 of these: 1GOKA and 1GOKB, 1GOM, 1I1XA, 1GOO and 1VBR [21, 30, 31]. The first 4 entries derive from the thermophilic fungus *Thermoascus aurantiacus*, while the final entry derives from the hyperthermophilic anaerobic bacterium *Thermotoga maritima*. These PDB entries as GH10 members possess high levels of sequence as well as structural similarities. As Table II shows, the *T. aurantiacus* xylanases with 2350 non-hydrogen atoms, display RMSDs of approximately  $0.5\text{\AA}$  in their three-dimensional conformations. For 1GOKA and 1GOKB, this RMSD is due to the different orientation of a small number of sidechains, while the RMSDs between the different crystal structures, 1GOK, 1GOM, 1I1X, and 1GOO, are due to slight structural differences distributed across the entire molecule. Even the structure from the hyperthermophilic bacterium, 1VBR, with 2700 non-hydrogen atoms, which obtains a sequence similarity score of 35% to 1GOKA, obtains a RMSD fit of  $1.06\text{\AA}$  and scores a structural alignment score of 92% to 1GOKA [32], emphasizing the structural similarity of these xylanases across species. Of the 5 PDB entries studied, the 1GOO computations included a ligand, glycerol, in the active site pocket at subsite -1.

PDB ID	1GOKA	1GOKB	1GOM	1I1XA	1GOO	1VBR
1GOKA	302	0.43	0.41	0.48	0.38	1.06
1GOKB	100	302	0.60	0.67	0.43	1.07
1GOM	100	100	302	0.48	0.43	1.07
1I1XA	98	98	98	302	0.60	1.22
1GOO	100	100	100	98	302	1.07
1VBR	35	35	35	36	35	324

TABLE II: Similarities of the 5 PDB entries analyzed. RMSD values of all-atom matches recorded above the diagonal. For 1VBR RMSD values represent best fits after pairwise sequence matching that eliminates unmatched residues. Percentage of primary sequence identities recorded below the diagonal. Diagonal entries indicate the number of amino acid residues per entry. RMSD values provided by PyMol.

We first examine the flexibility signatures of PDB entry 1GOK in both its A and B isoforms. The structure of this 302 amino acid, 2350 nonhydrogen-atom, polymer was determined to  $1.14\text{\AA}$  resolution by Lo Leggio and coworkers [21]. Figure 1 presents its structure in a ribbon representation, demonstrating the classic  $(\alpha/\beta)_8$  fold of this enzyme. Looking at the structure from the catalytic face such that the N and C terminal regions meet near the top of the figure, places the ligand binding groove roughly along the horizontal axis. This perspective places the catalytic Glu 131 below and Glu 237 above the axis. A second axis running nearly perpendicular to the first becomes apparent in animations: this vertical axis runs from the top, between the noncovalently bound N and C terminal regions, between  $\beta$ -strands 1 and 8 and  $\beta$ -strands 3 and 4 to the bottom-most residue, Asp 100, at the start of the 3rd  $\beta\alpha$  helix. The point of intersection of these two axes in Fig. 1 marks the location of subsite -2.

The electron density of the 1GOK data revealed two approximately equal populations (A and B) in which 11 residues could adopt one of two conformations [21]. Their all-atom RMSD is  $0.43\text{\AA}$ . Upon inspection, it is seen that most of this difference is due to three residues adopting distinct conformations (Fig. 2). All three residues, Trp 275

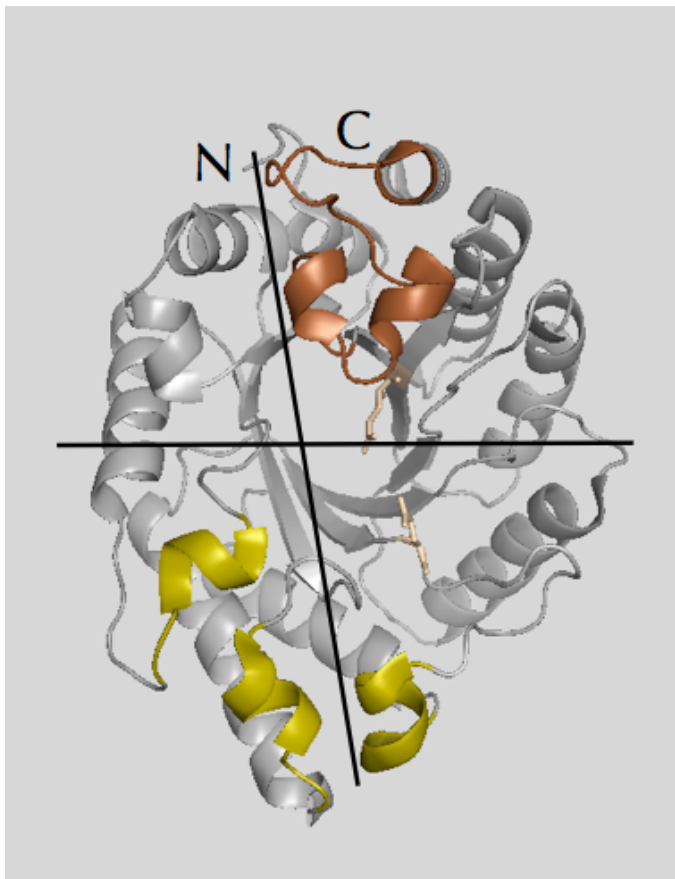


FIG. 1: Ribbon representation of 1GOK prepared using PyMol. The eight parallel  $\beta$ -strands of the TIM barrel open at the catalytic face where the catalytic glutamate sidechains are drawn as sticks. The binding groove runs roughly along the horizontal axis and separates the upper and lower domain motion evident in modes 1 and 2. The nearly vertical axis separates two vertical domains that likewise oppose eachother in modes 1 and 2. The C and N terminal regions meet at the top, the “mallet” region is highlighted in the upper right quadrant, while the three short helices composing “chin” region are highlighted in the lower two quadrants. Catalytic Glu 131 falls below the horizontal axis, while Glu 237 is above this axis.

(light green), its neighbor Arg 276 (dark green) as well as Glu 46 (red), line the binding groove about subsites -1 and -2, and are strictly conserved among GH10 members. The remainder of the binding groove residues, including the catalytic glutamates (magenta) as well as two arginines, 47 and 175 (yellow) known to promote enzyme-ligand association, are identically situated in the two isoforms. Indeed, excluding one sidechain, Trp 275, in calculating the all-atom RMSD between isoforms A and B reduces the fit from 0.43 to 0.27Å. If the side chains of all three residues, Trp 275, Arg 276 and Glu 46 are excluded in the RMSD computation, the overall fit further improves to 0.15Å.

In the 1GOK structures, Trp 275 in particular obtains an interesting position: at the end of the eighth  $\beta\alpha$ -loop of the TIM barrel, it projects down and over the subsite -1 hollow. The image of a lid comes to mind, an image that is re-inforced by the fact that Trp 275B seems to correspond to a “shut” and Trp 275A to an “open” orientation of the lid. The apparent lid-like opening and closing that Trp 275 effects is mediated by substantial shifts in the side chain dihedral values between isoforms A and B:  $(\chi_1, \chi_2) = (70^\circ, -61^\circ)$  in A and  $(-75^\circ, 38^\circ)$  in B. The effect is dramatic: atom CZ2 of Trp 275, for example, sweeps out an arc of nearly 8Å from the A to B conformation. To accommodate such substantial local fluctuation, the neighboring Arg 276 side chain likewise shifts to a substantial degree: its CZ atom shifts by 5Å from B to A conformers. And indeed, as pointed out by Lo Leggio and coworkers, Trp 275 in its A conformation sterically clashes with Arg 276 in its B conformation, making their assignments to population A or B unambiguous [21]. Intriguingly, no closed B conformations can be detected for Trp 275 or Arg 276 in structures solved with any type of ligand present in the binding groove.

We were interested to observe whether a PDB-NMA could detect differences in eigenspectra and concomitant eigenmotions due to the small but pertinent shifts of 3 residues out of 302 in this high resolution structure. [As we will show](#), we find a clear difference in the mobility spectra of 1GOKA and B: the closed, B conformation dampens the oscillatory behavior seen in the A conformation. To assess possible relevance of this difference, we next compute

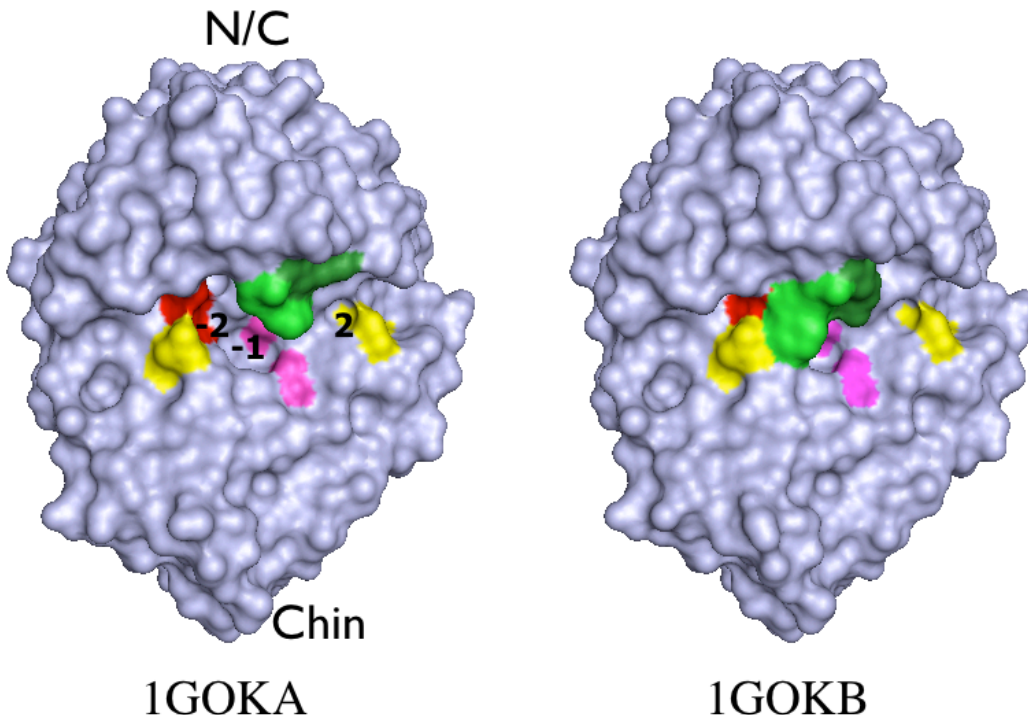


FIG. 2: Surface representations of 1GOK A (left), with the “open” orientation of Phe 275 and Arg 276 in green, and of 1GOK B, the “closed” conformation. The catalytic glutamates are colored magenta and Glu 46 in red. Arg 47 and Arg 175, colored yellow, are known to be involved in the primary binding interactions with substrates at subsites -2 and 2.

the flexibility spectra of *T. aurentiacus* xylanases 1GOM and 1I1X that also differ at the level of RMSD of 0.5Å, but due to delocalized structural differences. Again we observe clear and seemingly pertinent trends supporting our observations regarding the B conformation. We then assess whether the effects observed with Trp 275 and Arg 276 in their B form is emulated by the presence of a ligand in subsite -1 by computing the eigenmodes of 1GOO. We find that the presence of glycerol in the active site cleft does not effect the same dampening as in the B conformations of Trp 275 and Arg 276. Finally, we will compare the similarities in the flexibilities of fungal (1GOK) versus bacterial (1VBR) xylanases which further emphasize the possible relevance of observed trends.

### III. RESULTS

Table III shows results of the dihedral-based PDB-NMA on the PDB entries. 1GOKA and 1GOKB obtain 9413 vs. 9390 nonbonded interactions, with the closed, B, conformation losing 23 NBI due to loss of alignment of Trp 275 and Arg 276 with the 8th and 6th- $\beta\alpha$  loops of the TIM barrel as it swings shut over the subsite -1 cavity. This 0.25% decrease in the number of NBI results in an increase of nearly 9% from the slowest mode frequency of  $2.77\text{ cm}^{-1}$  for 1GOKA to  $3.02\text{ cm}^{-1}$  for 1GOKB. Activating the NS according to each eigenvector results in RMSDs of 0.38Å and 0.37Å for 1GOKA and B; nearly identical but slightly bigger for the “softer” open A isomer, despite the smaller  $C$  value. The surprise, however, is in the concomitant distribution and largest deviation from NS for all  $C_\alpha$ . In Fig. 3 we plot the RMSD from the NS of each  $C_\alpha$  due to thermal activation of the slowest mode for 1GOKA (blue) and B (orange). The curves closely overlap, as anticipated for two such similar structures, with a notable exception in the C terminal domain. The curves in Fig. 3 match closely until Trp 267, when the open A conformer suddenly obtains decidedly larger RMS values than those of the B isomer until Tyr 294 when the RMS values again match until the C terminal residue. The transition point, 267, occurs at the C terminal end of the eighth  $\beta$ -strand (residues 261-266) and belongs to one of the conserved tryptophan residues lining subsite -1. This differently mobile region extending from Trp 267 to Tyr 294 includes the lid residues Trp 275 and Arg 276, and is highlighted in the upper right quadrant in the ribbon representation of Fig. 1. We will refer to this region as the “mallet”. Interestingly, this particular loop structure, the mallet, seems to divide the members of GH10 xylanases into two subsets: molecules with (subset

2) or without (subset 1, like 1GOK) an additional  $\alpha$ -helical stretch immediately after the conserved Trp-275 or its equivalent [21]. Counterintuitively, but probably due to the loss of mobility of the B conformer at the C terminal region, this conformer, with slightly fewer NBI and a stiffer  $C$ , obtains a decidedly larger maximum deviation, at residue 100, than the closed conformer: 3.72Å for B vs. 3.23Å for A, a 15% shift. Asp 100 and the short helix-loop preceding it (92-99) as well as the two neighboring short  $\alpha$ -helical regions (50-58 and 142-149) are highlighted in the lower half of Fig. 1, and will be referred to as the “chin” region.

PDB entry	NBI (NBI / atom)	C	Eigenmode Number					
			1			2		
			$f$	RMSD	$\Delta R_{max}$	$f$	RMSD	$\Delta R_{max}$
1GOKA	9413 (3.62)	114	2.77	0.38	3.23	3.20	0.34	2.65
1GOKB	9390 (3.61)	117	3.02	0.37	3.72	3.39	0.32	2.55
1GOM	9457 (3.64)	105	2.87	0.37	3.20	3.38	0.34	2.83
1I1XA	9340 (3.60)	127	2.74	0.39	3.23	3.38	0.32	2.83
1GOO	9619 (3.70)	85	3.10	0.36	3.10	3.51	0.32	2.16
1VBR	10,407 (3.53)	98	2.49	0.38	3.54	2.85	0.34	2.95

TABLE III: Results of dihedral-based PDB-NMA on PDB entries. NBI gives the numbers of nonbonded interactions included for each computation, NBI/atom gives the average numbers of interaction per atom, and the constant  $C$  gives the overall scale factor. The frequencies  $f$  are given in units of  $cm^{-1}$ , the RMSD are computed for 180K over all atoms, and the maximum deviation of any atom from NS is given, in Å, under  $\Delta R_{max}$ .

We studied the mobility patterns via 3d animations to better understand the nature of the computed flexibilities. The slowest modes of 1GOKA are presented as GIF animations (using LICCap) in surface representations (prepared with PyMol) with the catalytic glutamates in magenta and the subsite -1 tryptophan triad in green in the folders MODE1 and MODE2 at [33] as well as a pair of stationary images in Fig. 5. The slowest mode of 1GOK presents as a “chomping” motion, Pacman-style, of the C and N terminal region above the horizontal axis of Fig. 1 relative to the region below this axis. The motion at first glance appears very similar for the 1GOKA and B isoforms, with a remarkable plasticity surrounding a pronouncedly stable core at the active site. The catalytic glutamates that remain at a steadfast 5.5Å separation, for example, seem enabled by a design scheme that deflects innate motility to other portions of the molecule. Rather than a motility scheme that compartmentalizes the motions into blocks with tidy divisions between “fixed” stability faces and  $\beta$ -barrels and highly flexible mobility faces, the “shock-absorption” is distributed throughout the molecule, with portions adjacent to the stability points deflecting any propensity to distortions to other regions. The net effect is remarkable stability for select nonlocal, nonbonded interactions in the face of “indiscriminate” thermal agitation.

Further inspection of the 3d animations also reveals, like the RMS plots, that isoform A obtains a more pronounced swinging of the mallet region than isoform B. Studying the motility pattern, it becomes clear that several features permit this mallet region to obtain such large yet stable RMS deviations. The residues immediately preceding the mobile region starting at Trp 267 belong to  $\beta$ -strand 8 (residues 261-266) which is firmly embedded and anchored by the  $\beta$ -barrel construction. The loop immediately preceding this  $\beta$ -strand, linking  $\beta$ -strand 8 to  $\alpha$ -helix 7 (residues 244 to 258), is further stabilized by a disulfide bridge linking the N terminal residue of  $\beta$ -strand 8, Cys 261, to the N terminal region of  $\alpha$ -helix 7 at Cys 255. The residues beyond the mobile region ending at Tyr 294 form a C-terminal  $\alpha$ -helix (residues 291-302) that is anchored between the N-terminal  $\alpha$ -helix (residues 5-13) on one side and the neighboring  $\alpha$ -helix 7 on the other side, and which is itself stabilized, as mentioned, by the disulfide bridge between residues 255 and 261. Together, these features “ground” the mobile 267-294 region, maintaining overall structural integrity even as this region itself executes sizeable RMS excursions. It is precisely this motion of the mallet which is hampered and dampened in isoform B.

The chin region, meanwhile, having the largest moment arm, sweeps out the largest arc and obtains the largest RMSD in both conformers. Inspecting the disposition of the residues of this region (Fig. 1), we note that the short  $\alpha$ -helix (residues 92-97) preceding the highly mobile Asp 100 might move *en masse* with the neighboring short  $\alpha$ -helix at 142-149 at the end of  $\beta$ -strand 4. In fact this does not happen in 1GOK as we see a clear tendency of these two

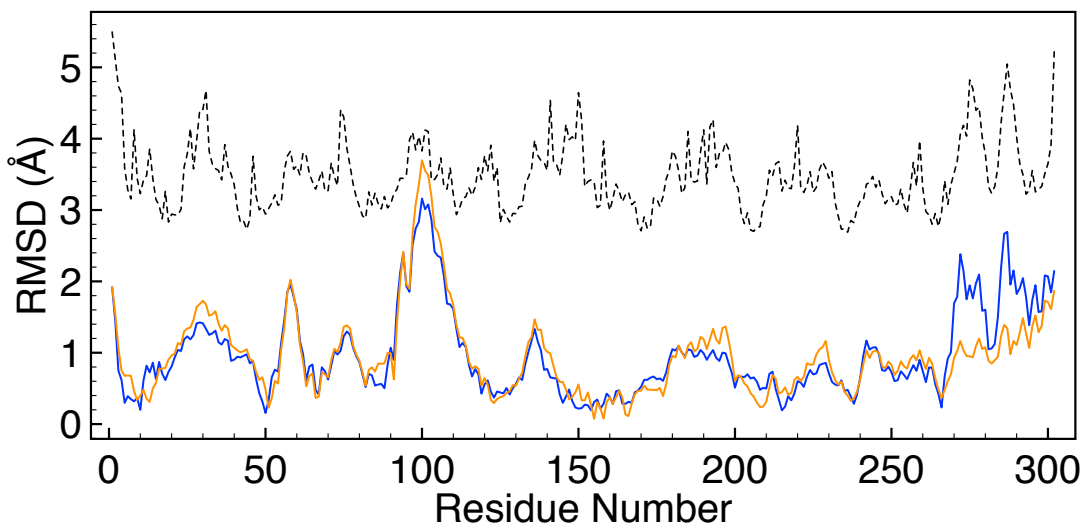


FIG. 3: RMSD for each  $C_{\alpha}$  due to mode 1 for 1GOKA (blue) and 1GOKB (orange). The average B factors for each residue, scaled to 10% the experimental values, are indicated by the dotted line.

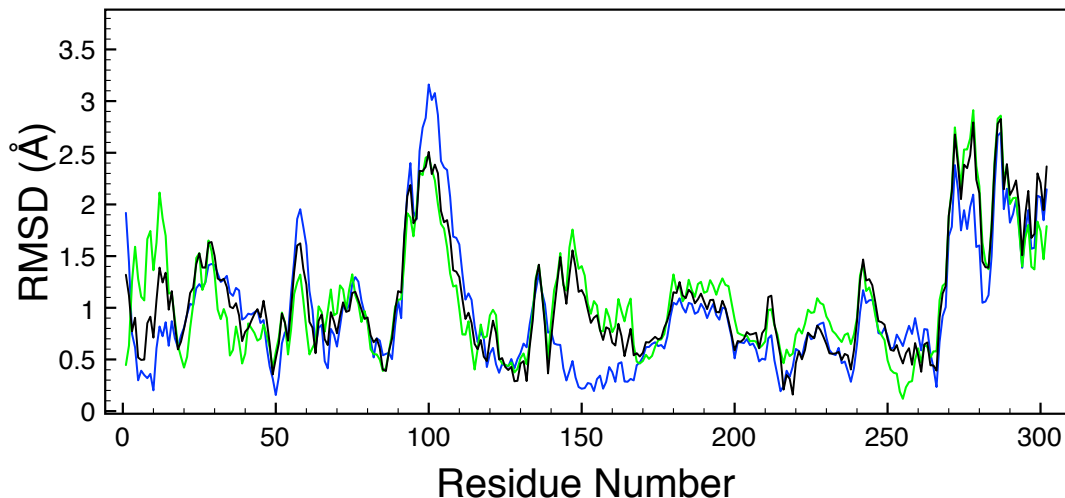


FIG. 4: RMSD for each  $C_{\alpha}$  due to mode 1 for 1GOKA (blue), 1GOM (green) and 1HIXA (black)

regions to pull apart. The mobile 92-100 chin region rather moves in tandem with the short  $\alpha$ -helix-loop above it, residues 50-58. The reason seems to be due to better stacking interactions between these two regions, including two indole rings. Trp 51 extends down from the upper, vertical helix of the chin, while Trp 94 is oriented upwards from the mobile 92-99 helix. This propensity of the  $\beta$ -strands 3 and 4 loops to pull away from each other mirrors that tendency between the C and N terminal domains, and creates the impression of a dynamic vertical axis, with residues on one side of the axis tending to pull away from residues on the other side. The point of intersection of these two axes is interesting, as residues Glu 46 and Gln 47, important ligand recognition and/or binding residues belonging to subsite -2, lie on one side of this divide, while Trp 275 and the other residues lining subsite -1 lie on the other side of this partition. This could result in a possible tension developing along an oligosaccharide spanning subsites -2 to +2, for example. In the motility pattern of 1GOKB, there is a decreased chomping over the horizontal axis, and an increased separation between the vertical domains due to the alignment of the indole ring of Trp 275 against Glu 46 and Gln 47. The net effect is a frustration of the chomping mode in 1GOKB and an increased propensity to distort the shape of subsite -2.

Interestingly, the experimentally observed B-factors of 1GOK, plotted as the dotted curve in Fig. 3, seem to suggest a large contribution from 1GOKA-type motility, with two peaks in the 267-294 region similar to those observed in the RMS plot of mode 1 of 1GOKA.



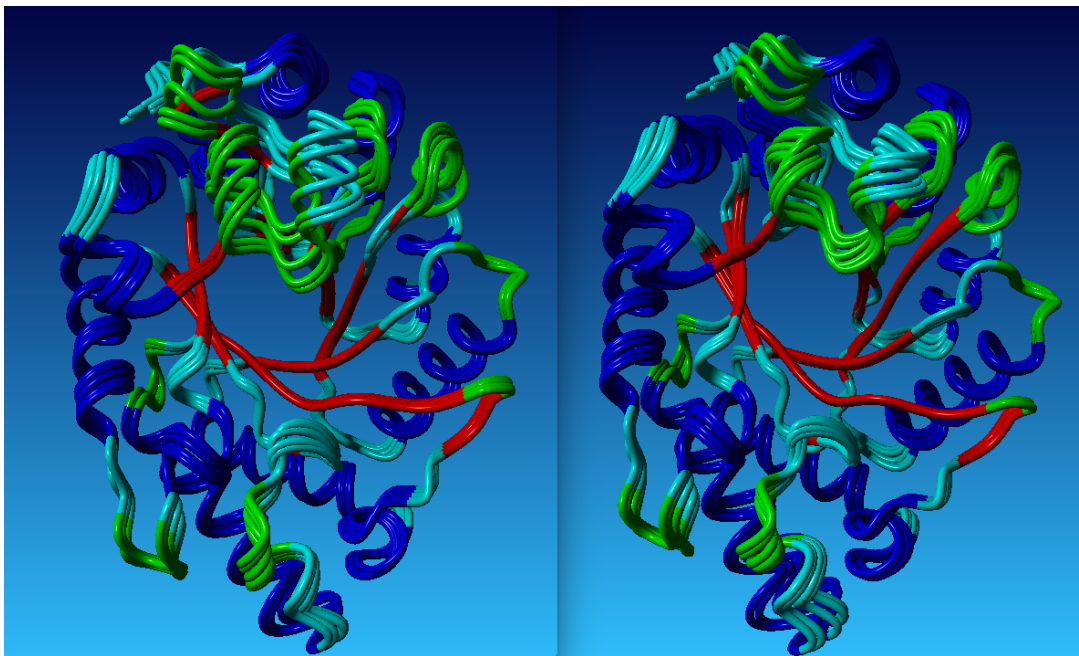


FIG. 5: Stationary images demonstrating the effects of modes 1 on 1GOKA (left) and 1GOKB (right). The images, prepared by YASARA, are in the orientation adopted in Figures 1 and 2 and show 5 different amplitudes of activation of mode 1 on the NS:  $\alpha_1 \sin(\frac{n\pi}{4})$ , with  $n=0, \dots, 4$ . The color scheme is by secondary structure, with sheets red, helices dark blue, turns green and coils light blue. Regions that remain stationary have closely overlapping elements, as for the 8 red  $\beta$  strands. Regions displaying greater motility present separated elements, especially noticeable in the mobile 267-294 region, the mallet, in the top center as green and light blue of each image. The mallet on the left, of the open 1GOKA, is oscillating far more than the one on the right, corresponding to the closed 1GOKB. These significantly differing signatures are due to the alternate orientations of merely 25 non-hydrogen atoms of Phe-275 and Arg-276, out of 2350 non-hydrogen atoms total, in the analysis. This presentation also provides a sense of the overall harmonicity of the motion, with the central NS structure straddled by the positive and negative amplitudes of activation of mode 1.

To test whether these differences in the presentation of mode 1 of 1GOKA and 1GOKB are significant, we compared their modes to those computed of two other molecules. One, 1GOM, is of the same protein but crystallized to a different crystal form (form I rather than II of 1GOK) and solved by Lo Leggio and coworkers to 1.94Å resolution [21]. 1GOM obtains a single conformation, equivalent to 1GOKA, and has an all-atom RMSD of 0.41Å compared to 1GOKA distributed equally over all residues: no single residue mismatches exist, except for a slight re-orientation of Trp 275. The other molecule we examined, 1I1X, is also of xylanase derived from a *T. auriantacus* strain, from Indian soil, and has a 297 out of 302 sequence-identity to 1GOK and 1GOM. The structure 1I1X was solved by Natesh and coworkers to 1.11Å resolution and obtained two conformers, A and B [30]. 1I1X crystallized to crystal form I, like 1GOM. The A and B conformers of 1I1X differ in the locations of 23 surface residues: all active site residues and ligand binding groove residues are resolved in one conformation, equivalent to the A conformer of 1GOK. We arbitrarily used 1I1XA for the current analysis, which obtained an all-atom RMSD fit to 1GOKA of 0.53Å, and to 1GOM of 0.48Å (Table II).

The number of NBI and C values used for computing the modes of these two proteins are provided in Table III. The frequency of the slowest mode of 1GOM is  $2.87 \text{ cm}^{-1}$  and of 1I1X is  $2.74 \text{ cm}^{-1}$ , similar to the value obtained for 1GOKA ( $2.77 \text{ cm}^{-1}$ ) whose open Trp 275 structure they resemble. The RMSD due to thermal activation of each  $C_\alpha$  atom in 1GOM is plotted in Fig. 4 (green), along with that of 1GOKA (blue). The curves demonstrate very similar mobility patterns, except for mismatches at residues 1-19, 140-168, and for the amplitudes for several peaks. Differences in these two curves may be due to the different crystal packing interactions or to the different resolutions of each model. We can ascertain which factor predominates by comparing the RMSD plot due to thermal activation of 1GOM to that of the other crystal form I structure, 1I1XA (black). Here we see that the  $C_\alpha$  deviations obtained by mode 1 of 1GOM are also obtained by 1I1XA, even though those structures differ by 0.48Å. The match includes the 140-168 region, the magnitudes of the peaks, and a tendency for the displacements of residues 1-19 toward those of 1GOM. In short, these curves demonstrate that in this case crystal packing effects more strongly correlate with thermal RMSD of the slowest mode than with resolution or with the precise details of the atomic orientations.

To further explore the possibility that Trp 275, by adopting the closed 1GOKB orientation, acts as a proverbial monkey wrench to block and frustrate the swing of the mallet region, we wondered whether another agent, namely

the presence of a ligand in subsite -1, in any way mimics the effects of this tryptophan. Lo Leggio and coworkers solved the structure of the crystal form II enzyme cryocooled to 100K [21]. A molecule of the cryoprotectant, glycerol, a mimic for xylose, was found at subsite -1, while Trp 275 and Asn 276 adopted the open conformation analogous to 1GOKA. How does the presence of this ligand affect the slowest mode? The PDB-NMA of 1GOO, including the additional 6 rigid-body degrees of freedom for the glycerol molecule, is unambiguous: the presence of glycerol in subsite -1 does not inhibit the “swings” of the mallet region in the way that Trp 275B does. The RMSD plot of each  $C_\alpha$  due to thermal activation of mode 1 (data not shown) shows that 1GOO obtains a motility spectrum much like 1GOM, with whom it shares an RMS fit of 0.51Å, including an active mallet region and a mobile N terminal domain. The presence of a small ligand in subsite -1 does not eliminate or frustrate the motion of the mallet region the way that Trp 275B does in 1GOK.

Finally, we examine the flexibility spectrum of a xylanase with an extra  $\alpha$ -helix after the Trp 275 loop, and therefore belonging to subset 2 of xylanases from GH10: 1VBR. The hyperthermophilic *T. maritima* xylanase 10B structure, 1VBR, was solved by Ihsanawati and coworkers to 1.8Å resolution as a dimer [31]. We used one copy from the dimer for our analysis. 1VBR obtains 324 residues and is therefore 22 residues longer than the other PDB entries analyzed. Superposing images of 1VBR and 1GOK reveals added residues in the loops after  $\beta$ -strands 8 (the Trp 275-equivalent loop) and 7, and at the end of the C terminal  $\alpha$  helix, lengthening that helix by 5 residues relative to 1GOK. Aside from these regions, the structural overlap between these two structures is excellent: 1GOK achieves a structural match of 98% to that of 1VBR, while their primary sequences obtain 35% identity (Table II).

The resulting slowest mode bears a striking resemblance, and is essentially identical, to that of 1GOKA, demonstrated by the stereo images available in the folder *1VBR + 1GOK<sub>M</sub>ODE1* at [33]. In this pair of GIF animations, green traces the mainchain of 1GOKA and cyan traces that of 1VBR. The sequence is presented in the customary frontal view equivalent to the orientation in Fig. 1 as well as from the side after rotation of 90° about a vertical axis.

The molecules move in tandem throughout the chain and throughout the sequence, and also obtain equivalent overall magnitudes of deformation; no additional parameterization was imposed to require comparable deviations. Clearly the architecture of the molecular chain selects for definite flexibility characteristics, irrespective of the particular primary sequence. These sequences also resolve a puzzle observed with subset 2 Family 10 xylanases: why the Trp 275- equivalent residues (802 in 1VBR) obtain relatively small temperature factors compared to their values among the subset 1 members. The active site Trps are not more disordered in subset 1 enzymes compared to those in subset 2, they are less mobile than the extended mallet region of these structures. In 1VBR, the mallet region once again starts at the Trp located at the C terminal end of  $\beta$ -strand 8 (residue 794) and extends to Tyr 826 in the C terminal  $\alpha$ -helix, but then obtains a further contribution from residues inserted in the loop sequence after  $\beta$ -strand 7: Arg 757-Gln 771. This latter region seem to “bulk up” one end of the mallet while the added residues in the C terminal helix seem to do the same for the obverse end of the mallet. It is interesting to note that the stabilizing disulfide bridge of 1GOK, located toward the stability face of that molecule, has moved in 1VBR. A cysteine located at the N-terminal end of  $\alpha$ -helix 8 (residue 825), is situated to potentially form a disulfide bridge with Cys 775 in the middle of  $\alpha$ -helix 7. In 1VBR however, the distance of separation of their respective SG atoms precludes the presence of this bond. In view of the fact that this molecule derives from a hyperthermophilic organism that thrives in 80C conditions, the absence of disulfide bridges is surprising.

#### IV. DISCUSSION

A number of interesting observations ensue from the study of the PDB-NMA signatures of subset 1 and 2 GH10 xylanases. Molecules that share a high degree of structural homology display equivalent flexibility characteristics, as seen in the slowest modes of 1GOKA, 1GOM, 1GOO, and 1VBR. The slowest mode pertains to a chomping motion and the second slowest mode pertains to a grinding motion across the ligand binding groove [10, 33]. Plots of RMS deviations from NS due to thermal activation as well as 3d animations of eigenvectors demonstrate that select residues remain largely immobile while other portions of the molecule display sizeable excursions about their NS. The OE2 atoms of the catalytic residues Glu 237 and Glu 131, for example, have a distance of separation of 5.57Å in the NS. Thermal activation of mode 1 in the current protocol suggests this distance may increase by 0.04Å or diminish by 0.11Å. In contrast, the neighboring subsite -1 residues Trp 275 and Trp 87 behave very differently. CE3 of Trp 275 is a distance of 8.45Å from CH3 of Trp 87 in the NS, and approach as close as 7.29Å and separate as far as 12.26Å, a net difference of nearly 5Å compared to a net difference of 0.15Å for the neighboring catalytic glutamates. It needs to be stressed that this criterion is not in any manner built into or required by the computation. This feature is an expression of packing constraints that uniquely define the internal symmetry axes of the molecule. The surprising immobility of key, nonbonded interactions permitted by the overall molecular design and resultant intra-molecular packing, may indeed have driven the selection of protein design.

While select NBI remain relatively immobile during thermal agitation, other regions display concerted movement,

such as the ligand binding groove and the C terminal mallet region. The substrate binding groove especially experiences considerable realignment. The slowest mode demonstrates an enhanced likelihood for the binding groove to be more and less solvent exposed as the N/C terminal, upper domain and lower domain close across the binding groove with a characteristic period of around 12 psec. In addition, the slowest mode reveals an interesting region that we refer to as the mallet, a region after  $\beta$ -strand 8 that obtains RMS shifts larger than other parts of the C/N domain. This particularly mobile region happens to segregate the GH10 members into two subsets depending on the nature of their loop design. Surprisingly, the mallet's motility is suppressed by the realignment of the indole ring of a *single* tryptophan, a realignment observed in the A and B conformers of the same crystal structure, 1GOK. What might be the consequences of such a mobile mallet region? A more thorough examination of the known GH10 structures might reveal connections between the size and mobility of this region and the nature of ligand bound, such as the degrees of polymerization and decoration for example.

And how to interpret the different Trp 275 orientations in light of these analyses? Experimental results demonstrate xylanase inactivation by oxidation of the active site tryptophan [34]. Furthermore, as pointed out, the X-ray crystallographic structure of the TIM-barrel GH enzyme, lysozyme, revealed that the oxidation and inactivation of its active site tryptophan resulted in a concomitant rotation of the indole moiety. This suggests a possibility that the 1GOKB structure represents an oxidized, inactive form of the enzyme. However, a different interpretation might be provided by the realignment of the active site tryptophan seen in lipases. Lipase activity is dependent on the orientation of a tryptophan residue in a surface loop, called the lid, being situated to either sterically hinder substrate access to the active site or to permit access to the active site [35]. A comparison of modes between these two enzymes might therefore prove of interest.

## V. CONCLUSION

PDB-NMA provides a direct, rapid and reproducible means to sensitively probe the flexibility signatures of PDB entries. The realignment of one or two residues out of 300 is sufficient to create distinct mobility spectra, and likely have direct biochemical consequences in terms of the activity or inactivity of enzymes, for example. On the other hand, PDB entries with a large degree of structural homology display very similar flexibility characteristics, even in the absence of a high degree of primary sequence homology.

We have examined primarily the slowest mode of several PDB entries. The shape of the slowest mode is principally due to the collective effect of thousands of nonbonded interactions and is therefore least sensitive to details in the potential energy formulation used to construct the eigenvalue equation. Higher frequencies probe greater details in the atomic potential and therefore require greater care in their formulation and computation. We here showed that the slowest eigenmode provides valuable insights into the unique flexibility characteristics of a particular molecular design, the TIM barrel fold in family 10 xylanases. We demonstrated that select NBI display little to no deformation under thermal agitation while other regions obtain large deformations. Observed flexibility patterns highlight regions that move *en masse* and bring into focus features removed from the active site that may nonetheless affect enzyme function. Efforts to correlate flexibility patterns and their timescales to enzyme functionality may enhance understanding of protein design.

## Acknowledgments

This work is supported in part by the M. Hildred Blewett Fellowship of the American Physical Society, <http://www.aps.org>.

- 
- [1] F. C. Bernstein, T. F. Koetzle, G. J. Williams, E. E. Meyer Jr., M. D. Brice, J. R. Rodgers, O. Kennard, T. Shimanouchi and M. Tasumi, "The Protein Data Bank: A computer-based archival file for macromolecular structures," *J. Mol. Biol.*, **112** 535 (1977).
  - [2] N. Go, T. Noguti and T. Nishikawa, "Dynamics of a small globular protein in terms of low-frequency vibrational modes," *PNAS* **80**, 3696-3700 (1983).
  - [3] B. Brooks and M. Karplus, "Harmonic dynamics of proteins: Normal modes and fluctuations in bovine pancreatic trypsin inhibitor," *PNAS* **80**, 6571-6574 (1983).
  - [4] M. Levitt, C. Sander and P. S. Stern, "Protein normal-mode dynamics: Trypsin inhibitor, crambin, ribonuclease and lysozyme," *J. Mol. Biol.* **181**, 423-447 (1985).

- [5] M. Levitt, C. Sander and P. S. Stern, "The Normal Modes of a Protein: Native Bovine Pancreatic Trypsin Inhibitor," *Int'l J. Quantum Chemistry: Quantum Biology Symposium* **10**, 181-199 (1983).
- [6] D. ben-Avraham and M. M. Tirion, "Dynamic and elastic properties of F-actin: A normal modes analysis," *Biophys. J.* **68**, 1231-45 (1995).
- [7] M. M. Tirion, "Large amplitude elastic motions in proteins from a single-parameter, atomic analysis," *Phys. Rev. Lett.* **77**, 1905 (1996).
- [8] H. Na and G. Song, "Bridging between normal mode analysis and elastic network models," *Proteins* **82**, 2157 (2014).
- [9] H. Na and G. Song, "Conventional NMA as a better standard for evaluating elastic network models," *Proteins* **83**, 259-267 (2014).
- [10] M. M. Tirion and D. ben-Avraham, "Atomic torsional modal analysis for high-resolution proteins," *Phys. Rev. E.* **91(3)** (2015).
- [11] I. Bahar, A. R. Atilgan, and B. Erman, "Direct evaluation of thermal fluctuations in protein using a single parameter harmonic potential," *Folding and Design* **2**, 173, (1997).
- [12] A. R. Atilgan, S. R. Durrell, R. L. Jernigan, M. C. Demirel, O. Keskin and I. Bahar, "Anisotropy of fluctuation dynamics of proteins with an elastic network model," *Biophys. J.* **80**, 505, (2001).
- [13] R. Mendez and U. Bastolla, "Torsional Network Model: Normal Modes in Torsion Angle Space Better Correlate with Conformation Changes in Proteins," *Phys. Rev. Lett.* **104** (2010).
- [14] M. E. Wall, R. Andreas, L. M. Rocha, "Singular value decomposition and principal component analysis," *A Practical Approach to Microarray Data Analysis* pp. 91-109, Kluwer: Norwell, MA (2003).
- [15] L. Skjaerven, A. Martinez and N. Reuter, "Principal component and normal mode analysis of proteins; a quantitative comparison using the GroEL subunit," *Proteins* **79(1)**,232, (2011).
- [16] T. Collins, C. Gerday and G. Feller, "Xylanases, xylanase families and extremophilic xylanases," *FEMS Microbiol. Rev.* **29**, 3-23 (2004).
- [17] B. Höcker, C. Jürgens, M. Wilmanns and R. Sterner, "Stability, catalytic versatility and evolution of the  $(\beta\alpha)_8$ -barrel fold," *Current Opinion in Biotechnology* **12**, 376-381 (2001).
- [18] C. S. Rye and S. G. Withers, "Glycosidase mechanisms," *Current Opinion in Chemical Biology* **4**, 573-580 (2000).
- [19] S. J. Charnock, T. D. Spurvey, H. Xie, M.-H. Beylot, R. Virden, R. A. J. Warren, G. P. Hazlewood and H. J. Gilbert, "The topology of the substrate binding clefts of glycosyl hydrolase family 10 xylanases are not conserved," *J. Biol. Chem.* **273(48)**, 32187-32199 (1998).
- [20] A. Moreau, F. Shareck, D. Kluepfel and R. Morosoli, "Alteration of the cleavage mode and of the transglycosylation reactions of the xylanase A of *Streptomyces lividans* 1326 by site-directed mutagenesis of the Asn173 residue," *Eur. J. Biochem.* **219**, 261-266 (1994).
- [21] L. L. Leggio, S. Kalogiannis, K. Eckert, S. C. M. Teixeira, M. K. Bhat, C. Andrei, R. W. Pickersgill and S. Laresen, "Substrate specificity and subsite mobility in *T. aurantiacus* xylanase 10A," *FEBS Letters.* **509**, 303-308 (2001).
- [22] M. Roberge, F. Shareck, R. Morosoli, D. Kluepfel and C. Dupont, "Characterization of active-site aromatic residues in xylanase A from *Streptomyces lividans*," *Protein Engineering* **12(3)**, 251-257 (1999).
- [23] H. K. Privett, G. Kiss, T. M. Lee, R. Blomberg, R. A. Chica, L. M. Thomas, D. Hilvert, K. N. Houk and S. L. Mayo, "Iterative approach to computational enzyme design," *PNAS*, **109(10)**, 3790-5 (2012).
- [24] C. C. F. Blake, R. Cassels, C. M. Dobson, F. M. Poulsen, R. J. P. Williams, K. S. Wilson, "Structure and binding properties of hen lysozyme modified at tryptophan 62," *J. Mol. Biol.* **147(1)**, 73-95 (1981).
- [25] J. M. Word, S. C. Lovell, J. S. Richardson and D. C. Richardson, "Asparagine and glutamine: Using hydrogen atom contacts in the choice of sidechain amide orientation," *J. Mol. Biol.* **285**, 1735-1747 (1999).
- [26] M. Levitt, "Molecular dynamics of native protein. I. Computer simulation of trajectories," *J. Mol. Biol.* **168**, 595-620 (1983).
- [27] M. Levitt, M. Hirshberg, R. Sharon and V. Daggett, "Potential energy function and parameters for simulations of the molecular dynamics of proteins and nucleic acids in solution," *Comp. Phys. Communication* **91**, 215-231 (1995).
- [28] H. Na, G. Song and D. ben-Avraham, "Universality of Vibrational Spectra of Globular Proteins" *arXiv* (2015).
- [29] D. Ringe and G. A. Petsko, " 'The glass transition' in protein dynamics: What it is, why it occurs, and how to exploit it," *Biophys. Chem.* **105**, 667-680 (2003).
- [30] R. Natesh, K. Manikandan, P. Bhanumorthy, M. A. Viswamitra and S. Ramakumar, "Thermostable xylanase from *Thermotoga maritima* at ultrahigh resolution (0.89Å) at 100K and atomic resolution (1.11Å) at 293K refined anisotropically to small-molecule accuracy," *Acta Cryst. D.* **59**, 105-117 (2003).
- [31] Ihsanawati, T. Kumasaka, T. Kaneko, C. Morokuma, R. Yatsunami, T. Sato, S. Nakamura and N. Tanaka, "Structural basis of the substrate subsite and the highly thermal stability of xylanase 10B from *Thermotoga maritima* MSB8," *Proteins* **61(4)**, 999-1009 (2005).
- [32] A. Prli; S. Bliven; P. W. Rose; W. F. Bluhm; C. Bizon; A. Godzik; P. E. Bourne, "Pre-calculated protein structure alignments at the RCSB PDB website" *Bioinformatics* **26**, 2983-2985 (2010).
- [33] <http://adweb.clarkson.edu/~mmtirion/>.
- [34] E. M. Woolridge, "Mixed Enzyme Systems for Delignification of Lignocellulosic Biomass," *Catalysts* **4**, 1-35 (2014).
- [35] A. Bourbon-Freie, R. E. Dub, X. Xiao and M. E. Lowe, "Trp-107 and Trp-253 Account for the Increased Steady State Fluorescence That Accompanies the Conformational Change in Human Pancreatic Triglyceride Lipase Induced by Tetrahydrolipstatin and Bile Salt," *J. Biol. Chem.* **284(21)**, 1417-14164 (2009).